Title

Establishing an Autonomous Cascaded Artificial Dynamic (AutoCAD) regulation system for improved pathway performance.

Authors

Jiang, Tian
Zou, Yusong
Zhang, Jianli
et al.

Publication Date

2022-11-01

DOI

10.1016/j.ymben.2022.08.009

Peer reviewed

HHS Public Access

Author manuscript

Metab Eng. Author manuscript; available in PMC 2024 March 18.

Published in final edited form as:

Metab Eng. 2022 November ; 74: 1–10. doi:10.1016/j.ymben.2022.08.009.

Establishing an Autonomous Cascaded Artificial Dynamic (AutoCAD) Regulation System for Improved Pathway Performance

Tian Jiang[1], **Chenyi Li**[1], **Yusong Zou**[1], **Jianli Zhang**[1], **Qi Gan**[1], **Yajun Yan**[1,*]

[1]School of Chemical, Materials, and Biomedical Engineering, College of Engineering, The University of Georgia, Athens, GA, 30602, USA

Abstract

Endogenous metabolic pathways in microbial cells are usually precisely controlled by sophisticated regulation networks. However, the lack of such regulations when introducing heterologous pathways in microbial hosts often causes unbalanced enzyme expression and carbon flux distribution, hindering the construction of highly efficient microbial biosynthesis systems. Here, using naringenin as the target compound, we developed an Autonomous Cascaded Artificial Dynamic (AutoCAD) regulation system to automatically coordinate the pathway expression and redirect carbon fluxes for enhanced naringenin production. The AutoCAD regulation system, consisting of both intermediate-based feedforward and product-based feedback control genetic circuits, resulted in a 16.5-fold increase in naringenin titer compared with the static control. Fed-batch fermentation using the strain with AutoCAD regulation further enhanced the naringenin titer to 277.2 mg/L. The AutoCAD regulation system, with intermediate-based feedforward control and product-triggered feedback control, provides a new paradigm of developing complicated cascade dynamic control to engineer heterologous pathways.

Keywords

cascaded dynamic regulation; biosensor; naringenin; *p*-coumaric acid; genetic circuit

Introduction

Sophisticated regulation networks in endogenous microbial metabolisms coordinate the intracellular gene expression and adapt cells to complicated conditions (Hengge-Aronis, 2002; Kochanowski et al., 2017; Lucchetti-Miganeh et al., 2008; Tani et al., 2002). In metabolic engineering, tailoring heterologous biosynthetic pathways into microbial

*Correspondence: yajunyan@uga.edu.

Author contribution

Tian Jiang: Conceptualization, Methodology, Investigation, Validation, Formal analysis, Data Curation, Writing Original Draft. Chenyi Li: Validation, Data Curation, Investigation. Yusong Zou: Methodology, Investigation. Jianli Zhang and Qi Gan: Investigation. Yajun Yan: Conceptualization, Supervision, Project administration, Resources, Funding acquisition, Writing Review & Editing.

Competing interest statement

The authors declare no competing financial interest.

hosts can cause unfavored distribution of metabolic fluxes and sub-optimal production performance, as such pathways often lack appropriate regulations (Li et al., 2021; Teng et al., 2022; Wang et al., 2021a). To solve this problem, dynamic pathway regulation has been developed to remedy the defect and improve the microbial biosynthesis (Doong et al., 2018; Farmer and Liao, 2000; Gupta et al., 2017; Li et al., 2022; Xu et al., 2014; Yang et al., 2018; Zhang et al., 2012). While single layer dynamic regulations have been demonstrated efficient in reducing the toxic intermediate accumulation (Dahl et al., 2013; Zhou et al., 2018) and minimizing competition between cell growth and production (Liu et al., 2019; Zhao et al., 2017), such regulation can become ineffective when facing complicated situations, as the single layer dynamic regulations only harbors one control logic which cannot be applied to multiple regulation targets. Therefore, multi-layer dynamic pathway regulation combining different control logic or utilizing multiple biosensors are required to enable precise and complex metabolic control, especially when regulating complicated biosynthetic pathways with multiple targets need to be controlled. Nonetheless, owing to the challenges such as low robustness, high cellular stochasticity, and potential crosstalk in multi-sensor systems, only a limited number of multi-layer dynamic regulation approaches in improving microbial biosynthesis have been reported so far (Dinh and Prather, 2019; Liang et al., 2020; Zhou et al., 2021).

As a complicated pathway with multiple biosynthetic steps, naringenin synthesis was largely used as a demonstration to explore the effect of multi-layer dynamic regulation. Naringenin is a plant-derived flavonoid with antibacterial, antifungal, and antiviral properties (Wang et al., 2019; Xiu et al., 2017; Yan et al., 2005). It was also explored in potential treatment for Alzheimer's disease (Ghofrani et al., 2015). The biosynthesis of naringenin has been achieved in *Escherichia coli* (*E. coli*), *Saccharomyces cerevisiae*, and other microorganisms (Lv et al., 2019; Palmer et al., 2020; Santos et al., 2011). The biosynthetic pathway of naringenin consists of four key enzymes: tyrosine ammonia lyase (TAL), 4-coumaryl-CoA ligase (4CL), chalcone synthase (CHS), and chalcone isomerase (CHI) (Fig. 1A) (Chouhan et al., 2017). The synthesis of naringenin suffers from multiple rate-limiting steps and the shortage of precursor supplies. Diah et al. developed a quorum sensing-based regulation system to dynamically control the expression of TAL and 4CL. Through dynamically delayed expression of TAL and 4CL, the naringenin titer increased to 204 μM (55.5 mg/L) (Dinh and Prather, 2019). However, as the cell growth state may not perfectly reflect the status of naringenin biosynthesis, using cell density as the signal to regulate naringenin biosynthesis may result in a sub-optimal timing of regulation. In a more recent example, Zhou et al. designed a multi-layered dynamic regulation system which mainly involved the multi-dimensional balancing of malonyl-CoA supply. The final naringenin titer, after multiple rounds of screening and optimization, reached 523.7 mg/L with the addition of 3 mM (544 mg/L) tyrosine, a direct precursor of naringenin biosynthesis (Zhou et al., 2021). While the naringenin production is encouraging, the inherent metabolic congestion caused by imbalance of enzyme expression in the naringenin pathway was not tackled.

Thus, in this study, we developed an Autonomous Cascaded Artificial Dynamic (AutoCAD) regulation system mimicking the natural regulation in cells to automatically fine-tune the enzyme expressions in naringenin pathway. The AutoCAD regulation system, composed of both intermediate-based feedforward and product-based feedback control genetic

circuits, resulted in balanced enzyme expression and improved biosynthesis performance. *p*-Coumaric acid responsive feedforward circuits were used to control the expression of rate-limiting enzymes (4CL and CHS) and resulted in a 10.4-fold increase (from 12.1 mg/L to 125.8 mg/L) in naringenin titer. Then, the naringenin-triggered feedback regulation circuit was integrated to further increase the expression of the key enzyme (CHS), which enhanced the naringenin titer to 148.3 mg/L. Further implementation of the *p*-coumaric acid-based feedforward regulation directed more malonyl-CoA for naringenin synthesis and increased the naringenin titer to 200.02 mg/L in shake flasks, demonstrating a 16.5-fold increase compared to the original strain without AutoCAD regulation system. The best performer harboring the AutoCAD regulation system was tested in fed-batch fermentation, and the highest *de novo* titer of naringenin was achieved to 277.2 mg/L. Our results demonstrated the necessity and efficiency of developing multi-function cascaded dynamic pathway regulations in microbial biosynthesis for mimicking natural regulation to enable high production of valuable compounds. The concept of AutoCAD regulation system that contains both intermediate-based feedforward control and product-triggered feedback control can also be applied in more biosynthetic pathways to dynamically and efficiently relieve the metabolic congestions, improve the efficiency of rate-limiting steps, and enhance the supply of precursors when needed.

Methods and materials

Plasmids, strains, and chemicals

Luria-Bertani (LB) medium containing 10 g/L tryptone, 5 g/L yeast extract and 10 g/L NaCl was used in this study for cell preculture. M9Y medium, which contained 20 g/L glycerol, 5 g/L yeast extract, 1 g/L NH_4Cl, 6 g/L Na_2HPO_4, 3 g/L KH_2PO_4, 0.5 g/L NaCl, 246.5 mg/L $MgSO_4$ $7H_2O$ and 14.7 mg/L $CaCl_2$ $2H_2O$, was used for naringenin biosynthesis. *E. coli* XL1-Blue was used for plasmid construction and *E. coli* BW25113 (F') was used for characterizing the dynamic performance of the biosensor system. The *pheA* and *tyrR* were knocked out in the genome of *E. coli* BW25113 (F') to construct the strain *E. coli* BW25113 (F') Δ*pheA*Δ*tyrR* in our previous study (Wang et al., 2017). The strain TJ1 was constructed by integrating the pLlacO1-controlled CHI operon to the *dkgB* locus in the genome of *E. coli* BW25113 (F') Δ*pheA*Δ*tyrR* through homologous recombination. IPTG was used for enzyme induction with a final concentration of 0.5 mM. The antibiotics kanamycin and ampicillin were added into the medium if needed to final concentrations of 50 μg/mL and 100 μg/mL, respectively. All the plasmids and strains used in this paper were listed in Table S1.

DNA manipulation and dynamic regulation circuits construction

The plasmids constructed in this paper were listed in Table S1. Three regulator plasmids Pcs-lpp0.2-PadR (WT), pCS-lpp0.2-PadR (K64A), and pZE-P9-egfp were constructed in our previous research (Jiang et al., 2021). The plasmid pHA-MCS containing a ColE1 origin, an ampicillin resistance gene, pLlacO1 promoter, and T1 terminator, was constructed in our lab based on previous study. The plasmid also carries a synthetic multi-cloning site (MCS) that sequentially contains the recognition sites of Acc65I, NdeI, BsrGI, SalI, ClaI, HindIII, NheI, BamHI, and MluI (Lutz and Bujard, 1997). To test the CHS conversion

efficiency, the plasmids pHA-PhCHS, pHA-Ra1CHS, pHA-Ra2CHS, pHA-PcCHS, were constructed by inserting four CHS genes into pHA-MCS using Acc65I and SalI. 4CL gene was inserted into the plasmids using AvrII and MluI to form plasmids pHA-PhCHS-4CL, pHA-Ra1CHS-4CL, pHA-Ra2CHS-4CL, pHA-PcCHS-4CL. The plasmid pCS-CHI was constructed by inserting CHI into pCS27 using Acc65I and SalI. To construct the plasmids for naringenin *de novo* synthesis, PhCHS was first inserted into pZE-lpp0.5-egfp (Li et al., 2022) using Acc65I and MluI, and 4CL was inserted into pZE-lpp0.5-egfp using Acc65I and XbaI. The lpp0.5–4CL operon was amplified and cloned into pZE-lpp0.5-PhCHS to obtain the plasmid pZE-lpp0.5-PhCHS-lpp0.5–4CL. The plasmid pCS-lpp0.5-TAL was constructed by inserting lpp0.5 promoter and TAL gene into pCS27 using XhoI, Acc65I, and BamHI. Site-directed mutation of PadR was conducted by overlap extension PCR using plasmid pCS-lpp0.2-PadR (WT) as template to form the plasmids pCS-lpp0.2-PadR (K127Y), pCS-lpp0.2-PadR (K127R), pCS-lpp0.2-PadR (H154W), and pCS-lpp0.2-PadR (H154R). For single-function feedforward control, pZE-P9–4CL was constructed by replacing egfp in pZE-P9-egfp with 4CL using Acc65I and XbaI. The plasmid pZE-lpp0.5-PhCHS-P9–4CL was constructed by inserting P9–4CL operon into pZE-lpp0.5-PhCHS using NdeI and AvrII. The regulator plasmids pCS-lpp0.5-TAL-lpp0.2-PadR (WT), pCS-lpp0.5-TAL-lpp0.2-PadR (K64A), and pCS-lpp0.5-TAL-lpp0.2-PadR (K127Y) were constructed by inserting lpp0.2-PadR (WT), lpp0.2-PadR (K64A), lpp0.2-PadR (K127Y) into pCS-lpp0.5-TAL, respectively. For dual-function feedforward control, pZE-P9-PhCHS was constructed by replacing egfp in pZE-P9-egfp with PhCHS using Acc65I and NdeI. The operon P9–4CL was inserted into pZE-P9-PhCHS using NdeI and BsrGI. For integration of feedback control of PhCHS on dual-function feedforward control circuit, we first constructed the plasmids of FdeR-P_{fdeA} biosensor system. The plasmid pZE-P_{fdeA}-egfp was constructed by replacing pLacO1 promoter in pZE-pLlacO1-egfp with P_{fdeA} promoter using XhoI and EcoRI. FdeR gene controlled by lpp1.0 was inserted into pCS-lpp1.0-egfp by using Acc65I and BamHI (Wang et al., 2017). The plasmid pZE-Pf_{deA}-PhCHS was constructed by replacing egfp with PhCHS using Acc65I and XbaI. The plasmid pZE-P9-PhCHS-P9–4CL-P_{fdeA}-PhCHS was constructed by inserting P_{fdeA}-PhCHS operon into pZE-P9-PhCHS-P9–4CL using BsrGI and AvrII. As the static control of the feedback control of PhCHS, pZE-P9-PhCHS-P9–4CL-lpp0.5-PhCHS was constructed by inserting lpp0.5-PhCHS operon into pZE-P9-PhCHS-P9–4CL using BsrGI and AvrII. The regulator plasmids pCS-lpp0.5-TAL-lpp0.2-PadR (WT)-lpp1.0-FdeR, pCS-lpp0.5-TAL-lpp0.2-PadR (K64A)-lpp1.0-FdeR, and pCS-lpp0.5-TAL-lpp0.2-PadR (K127Y)-lpp1.0-FdeR were constructed by inserting lpp1.0-FdeR and lpp0.2-PadR (WT) / PadR (K64A) / PadR (K127Y) operons into pCS-lpp0.5-TAL using SpeI, SacI, BspHI, XhoI sequentially. To dynamically improve malonyl-CoA supply, the plasmids pZE-P9-PhCHS-P9–4CL-P_{fdeA}-PhCHS-P_{fdeA}-asfabD and pZE-P9-PhCHS-P9–4CL-P_{fdeA}-PhCHS-P9-asfabD were constructed by inserting P_{fdeA}-asfabD and P9-asfabD operon into pZE-P9-PhCHS-P9–4CL-P_{fdeA}-PhCHS using AatII and SalI, respectively. The plasmids pZE-P_{fdeA}-asfabD and pZE-P9-asfabD were constructed by inserting *asfabD* into plasmids pZE-P_{fdeA}-egfp and pZE-P9-egfp using Acc65I and XbaI, respectively.

Characterizing the dynamic performance of biosensor system

The *E. coli* BW25113 (F') was used for characterizing the dynamic performance of the biosensors. Three independent transformants were randomly picked and cultivated in 3.5

mL LB medium with appropriate antibiotics. The seeds were incubated at 37 °C with a shaking speed at 270 rpm in the New Brunswick Excella E24 shaker for around 12 h. 150 μl seeds were transferred into 3.5 mL LB medium. When OD_{600} reached around 0.4 (roughly after 1h of cultivation), different concentrations of inducers/effectors were added into the medium. After 12 h of cultivation, all cultures were sampled to measure the fluorescence intensity and cell density, for which the Synergy HT plate reader from Biotek was used. The samples were diluted by 5 times (40 μL sample with 160 μL DI water) and transferred into a 96-well plate (Corning® 96-well Flat Clear Bottom Black Polystyrene TC-treated Microplates, Corning 3603). The green fluorescence intensity was detected by using an excitation filter of 485/20 nm and an emission filter of 528/20 nm. The green fluorescence intensities were normalized with the corresponding cell densities to calculate the unit egfp expression levels (RFU/OD_{600}).

Fermentation experiments

To determine the activity of different CHS, the plasmids pHA-PhCHS-4CL, pHA-Ra1CHS-4CL, pHA-Ra2CHS-4CL, and pHA-PcCHS-4CL were co-transformed with pCS-CHI into *E. coli* BW25113 (F'). The strains were cultivated in 3.5 mL LB medium at 37 °C for 10 h. 1 mL precultured strains were transferred into 125 mL shake flask containing 20 mL M9Y medium and incubated at 37 °C with 270 rpm. Isopropyl β-D-1-thiogalactopyranoside (IPTG) was added at a final concentration of 0.5 mM and *p*-coumaric acid was added with the final concentration of 400 mg/L after 2.5 h, then the strains were incubated at 30 °C with 270 rpm. Samples were taken after 24 h and 48h for OD_{600} determination and HPLC detection. OD_{600} was determined using the V-1200 spectrophotometer (VWR) with the pure water as a blank. The feeding experiments were performed in triplicates, and data are presented as the averages and standard deviations (n=3).

To explore the performance of dynamic regulation, related plasmids were transformed into strain TJ1. The strains were cultivated in 3.5 mL LB medium at 37 °C for 10 h. Then 1 mL precultured strains were transferred into 20 mL M9Y medium and cultivated at 37 °C for 2.5 h. IPTG was added with the final concentration of 0.5 mM to induce the expression of CHI in genome after 2.5 h, then the strains were incubated at 30 °C with 270 rpm. Samples were taken after 24 h and 48 h for OD_{600} determination and HPLC detection. OD_{600} was determined using the V-1200 spectrophotometer (VWR) with the pure water as a blank. The experiments were performed in triplicates, and data are presented as the averages and standard deviations (n=3).

Fed-batch fermentation

Fed-batch fermentation was conducted in 125 mL shake flask with 20 mL M9Y medium. The plasmids pZE-P9-PhCHS-P9–4CL-P_{fdeA}-CHS-P9-asfabD and pCS-lpp0.5-TAL-lpp0.2-PadR (K127Y)-lpp1.0-FdeR were co-transformed into TJ1. The strains were cultivated in 3.5 mL LB medium at 37 °C with 270 rpm. After 10 h, the precultured strains were transferred into 125 mL shake flask with 20 mL M9Y medium containing 20 g/L glycerol. After 2.5 h, IPTG was added to induce the expression of CHI in genome. Then the strains were cultivated in 30 °C with 270 rpm. Glycerol and yeast extract were supplemented

every 12 h after 24 h with the final concentration of 10 g/L and 5 g/L. The samples were taken after 4 h, 8 h, 12 h, 24 h, 36 h, 48 h and 60 h and prepared for HPLC detection. The experiments were performed in triplicates, and data are presented as the averages and standard deviations (n=3).

HPLC analysis

HPLC samples were prepared by adding methanol with the ratio of 1:1. After 15 min, the mixture was centrifuged with 12000 rpm for 5 minutes. Naringenin and *p*-coumaric acid concentration was analyzed by Agilent HPLC 1260 Infinity II (1260 Infinity II Diode Array Detector WR) with a reverse-phase ZORBAX SB-C18 column. For naringenin and *p*-coumaric acid detection, 0.1%TFA and methanol were used as the mobile phase at a flow rate of 1 mL/min. The analyzing method was set as follows: 5% methanol from 0–2 min, 5%−60% methanol from 2–25 min, 60%−90% methanol from 25–27 min, 90%−5% methanol form 27–29 min. Naringenin and *p*-coumaric acid can be detected at 26.53 min and 18.35 min, respectively. Glycerol concentration was analyzed by Dionex Ultimate 3000 (Ultimate 3000 Photodiode Array Detector) with a Coregel-64H column (Transgenomic). 4 mM H_2SO_4 was used as mobile phase at a flow rate of 0.40 mL/min. The oven temperature was set to 45 °C. Glycerol can be detected at 23.1 min.

Results

Diagnosis of the issues in naringenin biosynthesis

The naringenin pathway has been established in *E. coli* before by recruiting four enzymes, TAL from *Rhodotorula glutinis*, 4CL from *Petroselinum crispum*, CHI from *Medicago sativa*, and CHS from *Petunia hybrida* (Santos et al., 2011). The CHS was known to be a rate-limiting enzyme in this pathway (Zang et al., 2019).

To overcome this limitation, we tested four chalcone synthases, PhCHS, PcCHS, RaCHS1, and RaCHS2 from *Petunia hybrida*, *Polygonum cuspidatum*, and *Rheum austral*, respectively, along with 4CL and CHI. By feeding 400 mg/L *p*-coumaric acid, the strain harboring the PcCHS produced 2.1 mg/L of naringenin, which is extremely lower than the group of PhCHS (41.2 mg/L), while no naringenin production was detected in strains harboring RaCHS1 or RaCHS2 (Fig. 1B). These results confirmed the low conversion efficiency of the naringenin pathway, which was presumably due to both low enzyme activities and insufficient malonyl-CoA supply. We then selected the relatively more efficient PhCHS as the enzyme to construct the *de novo* naringenin biosynthetic pathway. To enhance the accumulation of tyrosine, the important precursor for *de novo* naringenin biosynthesis, we chose the strain *E. coli* BW25113 (F') Δ*pheA*Δ*tyrR* that was constructed in our previous study. As previously reported, CHI is highly efficient on converting naringenin chalcone to naringenin (Zang et al., 2019). Thus, to minimize the cellular burden, the expression cassette for CHI, was integrated into the genome of *E. coli* BW25113 (F') Δ*pheA*Δ*tyrR* at the *dkgB* locus, forming the final strain *E. coli*::*chi* Δ*pheA*Δ*tyrR* (TJ1). Further introduction of the moderately expressed TAL along with the highly expressed 4CL and PhCHS into the strain constitutes the platform strain for naringenin *de novo* biosynthesis. However, this strain only

accumulated 13.7 mg/L naringenin in shake flasks but accumulated 462 mg/L *p*-coumaric acid at 48 h (Fig. 1C).

The low pathway efficiency with high concentration of *p*-coumaric acid indicated a metabolic congestion. We hypothesized that this congestion was caused by constitutive and unbalanced enzyme expression, which may also bring increased metabolic burdens and result in poor production performance. The low catalytic efficiency of CHS and shortage of malonyl-CoA supply may also impair the high production of naringenin. Therefore, we reasoned that an AutoCAD regulation system consisting of both intermediate-based feedforward control and product-based feedback control can be designed to simultaneously address all these issues. Based on our analysis, *p*-coumaric acid-triggered feedforward control genetic circuits can be applied to dynamically fine-tune the expression of 4CL and CHS to relieve the cellular burdens from constitutive enzyme expression and balance the carbon flux distribution. Then, to address the low efficiency of CHS and inadequate malonyl-CoA supply, naringenin-based feedback control genetic circuits can be integrated to continuously strengthen CHS expression and enhance malonyl-CoA availability with the accumulation of naringenin. The combination of these regulation circuits forms the AutoCAD regulation system, which would contribute to a high production of naringenin.

Protein engineering improved the *p*-coumaric acid responsive biosensor

As we designed, a *p*-coumaric acid responsive biosensor was required to execute the artificial feedforward regulation. In our previous research (Jiang et al., 2021), a PadR-P_{padC} biosensor system responding to *p*-coumaric acid was established. In this biosensor system, the regulator PadR inhibits the expression of P_{padC}, but this inhibition can be released by *p*-coumaric acid (Fig. 2B). To further improve the sensitivity and dynamic range of this biosensor, we sought to rationally engineer the regulator PadR. The structure of the PadR from *Bacillus subtilis 168* was simulated with SWISS-Model (https://swissmodel.expasy.org/) using the crystal structure of PadR from *Bacillus subtilis subsp. spizizenii str. W23* (PDB ID: 5Y8T), a close homologous protein (with a sequence similarity of 98.4%), as the template (Park et al., 2017). There are two residues, R164 and H154, that directly interacting with the native substrate *p*-coumaric acid of PadR. The residue R164 can form two hydrogen bonds with the carboxylate group of *p*-coumaric acid while the H154 residue can only form one hydrogen bond with the *p*-coumaric acid. Thus, we hypothesized that the R164 was dominant in the ligand binding but the H154 may only perform an assisting role for recognizing the *p*-coumaric acid. Aside from the H154 and R164, one additional residue K127 that located at the right side of the substrate binding pocket but did not directly interact with the substrate, was also hypothesized to be critical in reshaping the binding pocket. We hypothesized that, by replacing the K127 to larger amino acids, especially those that would significantly reshape the binding pocket and push the substrate towards the H154, the substrate binding pocket would be narrowed, and it would likely improve the binding affinity between PadR and *p*-coumaric acid.

Our goal is to reduce the size of the substrate binding pocket to explore whether we can obtain PadR mutants with better sensitivities and dynamic ranges. To avoid potential loss-of-function mutations, we selected the H154, the assisting residue for *p*-coumaric acid

binding, as our first target rather than the residue R164 which is supposed to be more essential for *p*-coumaric acid binding. The H154 was substituted with larger amino acids to reduce the pocket size, resulting in PadR variants H154W and H154Y (Fig. 2A). The responsiveness of two rationally designed PadR mutants were tested using the previously constructed hybrid promoter P9, which exhibited increased strength compared to wild type P_{padC}, as the responding promoter (Jiang et al., 2021). However, these two variants were unable to recognize *p*-coumaric acid, which implied that the residue H154 was crucial for *p*-coumaric acid binding, though only one hydrogen bond was formed with *p*-coumaric acid (Fig. 2C). Based on this, we selected the residue K127 as our second target, because it does not directly interact with the substrate. Aiming to narrow the substrate binding pocket, the K127 was substituted with tyrosine (K127Y) or arginine (K127R) (Fig. 2A). As expected, *p*-coumaric acid can be recognized by both variants and release the repression, indicating the substitution of residue K127 can maintain the substrate binding. The highest responsive strength of PadR (K127Y) improved by 25% compared with PadR (WT) when induced with 600 mg/L *p*-coumaric acid (Fig. 2C).

In our previous study, we obtained an engineered PadR variant (K64A) with increased responsive range and strength toward *p*-coumaric acid by modifying its DNA binding domain (Jiang et al., 2021). However, the dynamic ranges of PadR (WT) and PadR (K64A) towards *p*-coumaric acid when using P9 promoter (the mutant of P_{padC} with increased strength) has not been characterized (Jiang et al., 2021). As the variant PadR (K127Y) also exhibited an increased responsive strength toward *p*-coumaric acid compared to PadR (WT), we sought to compare the dynamic ranges of PadR (WT, K64A, and K127Y) against *p*-coumaric acid with P9 as the promoter. In our test, both the PadR (K127Y) and PadR (K64A) enabled an expanded dynamic range compared to the PadR (WT), with 19% (K127Y) and 18% (K64A) increase in the responsive strength induced by 800 mg/L *p*-coumaric acid. The PadR (K127Y) was the most sensitive variant when induced by low *p*-coumaric acid concentrations (0–200 mg/L), with a 63% and 10% higher responsive strength (at 200 mg/L) than the PadR (WT) and PadR (K64A), respectively (Fig. 2D). The different dynamic properties may result in varied performance of the regulation circuits. Thus, all three PadR regulators were paired with promoter P9 to form the *p*-coumaric acid-responsive biosensor, which were used for constructing the AutoCAD regulation system and investigating how the dynamics of the biosensor would affect the performance of the system.

Feedforward control of 4CL expression to improve naringenin production

Based on the results of pathway diagnosis, the two major problems in naringenin biosynthesis were the low naringenin titer and relatively high accumulation of *p*-coumaric acid. As we analyzed, these problems were likely caused by the unregulated expression of heterologous enzymes, which resulted in the metabolic congestion and increased metabolic burdens. To solve this issue, we designed to first target the expression of the rate-limiting enzyme 4CL. Thus, an artificial feedforward control circuit was employed to dynamically regulate the expression of 4CL. The accumulation of *p*-coumaric acid signals the start of naringenin biosynthesis, and the *p*-coumaric acid-triggered feedforward control would gradually activate 4CL expression when the cells start to produce *p*-coumaric acid. Hence, this strategy would not only relieve the metabolic burdens by reducing the waste

of resources for unnecessary protein synthesis, but also dynamically enhance the 4CL expression to accelerate the consumption of *p*-coumaric acid. To this end, we placed the 4CL coding gene under the control of the promoter P9, while all other genes remain to be constitutively expressed (Fig. 3D). To ensure the precise control of feedforward regulation, we also confirmed that PadR and its mutants cannot respond to the intermediate tyrosine and the product naringenin (Fig. S2A and S2B). The static control groups also contain the corresponding regulator expression cassette (Fig. 3A).

With 4CL under the control of P9, the feedforward regulation circuit harboring the WT PadR drastically improved the naringenin titer to 102.6 mg/L, representing a 16.55-fold increase compared with the static regulation (6.2 mg/L) (Fig. 3B and E). Notably, the *p*-coumaric acid titer also exhibited a 2.79-fold increase from 268.3 mg/L to 747.5 mg/L (Fig. 3C and F), and a slight increase (9%) in cell densities was perceived after applying the dynamic regulation (Fig. 3B and E). Similar trends were observed in the circuits harboring the PadR (K64A) and PadR (K127Y). The naringenin titer was increased form 14.9 mg/L to 100.9 mg/L when the circuit was controlled by PadR (K64A), while the circuit harboring the PadR (K127Y) increased the naringenin titer from 12.1 mg/L to 105. 1 mg/L (Fig. 3B and E). When regulated by K64A and K127Y, *p*-coumaric acid concentration also increased by 1.64-fold and 1.84-fold, respectively, compared to the related static control (Fig. 3C and F). The feedforward regulation resulted in relived metabolic burdens and thus enabled a better cell growth. The increased *p*-coumaric acid titers also suggested that dynamic regulation of 4CL expression streamlined this heterologous pathway and directed more carbon source for naringenin synthesis. Notably, comparing with the regulation enabled by PadR (WT), the enhanced 4CL expression when controlled by PadR (K64A) or PadR (K127Y) only slightly increased the naringenin titer, which suggested that the *p*-coumaric acid-based feedforward circuit harboring the PadR (WT) was efficient to eliminate the metabolic burden from constitutive 4CL expression. Taken together, the introduction of feedforward regulation of 4CL expression can efficiently relieve the cellular burdens and increase the naringenin production.

Introducing feedforward control on CHS expression

To further reduce the cellular burdens on constitutive protein expression, we continued to apply the *p*-coumaric acid-responsive feedforward control circuit to regulate the PhCHS expression. The feedforward control would activate the expression of PhCHS when *p*-coumaric acid starts to accumulate, and the high concentration of *p*-coumaric acid would enhance the expression of this rate-limiting enzyme to drive the consumption of *p*-coumaroyl-CoA and reduce the overly accumulated *p*-coumaric acid. Thus, we anticipate the dual-function feedforward control circuit would further relieve the metabolic burden and enhance naringenin production.

To construct the dual-function feedforward control circuit, the constitutive promoter lpp0.5 controlling the expression of PhCHS was replaced by the P9 promoter, forming the plasmid pZE-P9-PhCHS-P9–4CL (Figure 3G). This plasmid was co-transferred with the plasmid pCS-lpp0.5-TAL-lpp0.2-PadR and its variant plasmids harboring the PadR (K64A) or PadR (K127Y), respectively. However, when regulated by PadR (WT), the naringenin only

accumulated to a titer of 64.5 mg/L after applying dual-function feedforward control (Fig. 3H), which was lower than what we observed when only controlling the 4CL (102.6 mg/L) (Fig. 3E). We also noticed an increase of *p*-coumaric acid concentration from 747.5 to 874.4 mg/L (Fig. 3F and I). A similar trend was observed when the feedforward control was enabled by PadR (K64A). The naringenin titer decreased from 100.9 mg/L to 88.9 mg/L (Fig. 3E and H), while the *p*-coumaric acid titer increased from 764.1 mg/L to 864.9 mg/L (Fig. 3F and I). In both cases, no significant change in the cell densities were observed after using dual-function feedforward control (Fig. 3F and I), which may indicate that the cellular burden from constitutive protein expression was minimal after applying single output feedforward control. Surprisingly, when the control circuit equipped with PadR (K127Y), the naringenin titer (125.8 mg/L) increased by 19.7% compared to the titer in the single-function feedforward control (105. 1 mg/L) (Fig. 3H and E), and the accumulation of *p*-coumaric acid only slightly increased (from 750.8 mg/L to 779.0 mg/L) (Fig. 3F and I). This was likely because that the dual-function feedforward control circuit with the more sensitive regulator PadR (K127Y) resulted in an earlier activation of PhCHS expression and thus enabled an increased naringenin titer, while the circuits harboring the less sensitive PadR regulators (WT and K64A) cannot boost the production. These results highlighted the importance of the timing of executing the dynamic pathway regulation. Nonetheless, the increase in naringenin production was less prominent compared with when the expression of 4CL was changed from “static” to “dynamic”, which indicated that the metabolic burdens from constitutive enzyme expression was no longer a major problem hindering the improvement of naringenin production after the feedforward regulation. The naringenin titer enabled by PadR (K64A)-controlled circuit was slightly higher (88.9 mg/L vs 64.5 mg/L) than that of the PadR (WT)-controlled circuit (Fig. 3H), which was likely because the responsive strength enabled by PadR (K64A) was higher than that of the PadR (WT) (Fig. 2D). These results suggested that the increased expression of PhCHS would contribute to a higher production of naringenin, which further indicated that the PhCHS, after the application of the dual-function feedforward control, was the key rate-limiting step for naringenin biosynthesis.

Integrating feedback control to increase the expression of rate-limiting PhCHS

As we concluded in the last section, the PhCHS remains to be a rate-limiting step in the naringenin pathway, which constrained the further improvement of naringenin biosynthesis. As the metabolic burdens were no longer the major problem, we sought to use product-triggered feedback control to continuously enhance the rate-limiting enzyme (PhCHS) expression with the production of naringenin. Such feedback loop can enable high expression level of PhCHS to supplement its low enzyme activity without introducing extra cellular burdens, as this circuit would enable low expression of CHS during early cell growth stage but allow high PhCHS expression when the cells enter to production phase. To this end, a biosensor responding to the final product naringenin is required. In previous studies, a biosensor system FdeR-P_{FdeA} was identified which could response to different concentrations of naringenin (Siedler et al., 2014; Wassem et al., 2017). In this biosensor system, only when both the regulator FdeR and the effector naringenin were present can the promoter P_{fdeA} be activated. We reconstructed this biosensor system in our study by replacing the promoter pLlacO1 in pZE-pLlacO1-egfp by P_{fdeA} to form

the reporter plasmid pZE-P_{fdeA}-egfp, and the regulator FdeR was controlled under the constitutive promoter lpp1.0 in pCS27 plasmid, resulting in plasmid pCS-lpp1.0-fdeR (SI Appendix, Fig. S1A) (Wang et al., 2021b). To apply this biosensor system in the AutoCAD regulation network, we first determined its dynamic range in *E. coli*. With the increase of naringenin concentration from 0–200 mg/L, the responsive strength of P_{fdeA} increased by 53.7-fold, which demonstrated the successful reconstruction of FdeR-P_{fdeA} biosensor system. However, the maximum responsive strength of the P_{fdeA} promoter only accounted for 41.2% and 31.8% of the activity of promoter P9 and lpp0.5, respectively (SI Appendix, Fig. S1B). Notably, there was a rapid increase in the responsive strength of the biosensor system at low concentrations of naringenin (0–50 mg/L), where the egfp expression level increased from 71.4 to 3081.3 a.u. (SI Appendix, Fig. S1A). These results indicated that the biosensor system was sensitive enough to turn on the downstream gene expression even at low naringenin concentration.

To explore whether the feedback control of PhCHS expression can efficiently compensate the low enzyme activity, an additional expression cassette of PhCHS controlled by P_{fdeA} and the constitutively expressed regulator FdeR was introduced into the dual-function feedforward control circuits harboring different PadR variants, resulting in three tri-function genetic circuits (Fig. 4A). To ensure there was no crosstalk in the system, the FdeR-based biosensor was tested against *p*-coumaric acid, and the results showed that *p*-coumaric acid cannot activate the naringenin-responsive biosensor (Fig. S2C). The integration of the feedback control enabled increased naringenin titers in all three tri-function circuits. The final naringenin titers were 100.8 mg/L (WT), 133.7 mg/L (K64A), and 148.3 mg/L (K127Y), which showed 1.56, 1.50, 1.18-fold increases compared to that of dual-function feedforward control circuits without the integration of feedback control on PhCHS expression (Fig. 4B and 3H). Notably, further applying the product-triggered feedback control on PhCHS expression enabled lower *p*-coumaric acid accumulations in tri-function circuits compared to when only the dual-function feedforward control circuits were applied (Fig. 4C and 3I). This was likely because the integration of feedback regulation pulled the consumption of *p*-coumaroyl-CoA for naringenin synthesis, and thus more *p*-coumaric acid was consumed. The different naringenin titers again highlighted the dynamic performance of the biosensor system can impact the effect of dynamic regulation.

We also want to test whether the feedback control can perform better than a static enhancement of PhCHS. Thus, the lpp0.5-controlled PhCHS expression cassette was integrated with three dual-function feedforward control circuits, which generated the static control (Fig. 4D). No significant change of the naringenin titers was observed compared to the feedback control on PhCHS when regulated by the PadR (WT) and PadR (K127Y) (Fig. 4B and E), and the concentrations of *p*-coumaric acid in dynamic groups were higher than in the static groups (Fig. 4C and F). The tri-function genetic circuit harboring the PadR (K64A) as regulator even enabled a higher naringenin titer (133.7 mg/L vs 118.1 mg/L) than that of the static control (Fig. 4E and B). These results again demonstrated the superiority of dynamic pathway regulation. Even with a promoter exhibiting a much lower activity (P_{fdeA} vs lpp0.5) (SI Appendix, Fig. S3), the dynamic feedback control can enable more efficient biosynthesis with a higher naringenin titer (Fig. 4C and F). Therefore, product-triggered dynamic feedback control, compared to constitutive enzyme expression,

can enable high expression of rate-limiting enzymes without introducing extra cellular burdens and subsequently increase the biosynthesis efficiencies.

Assembling the AutoCAD regulation network for improved naringenin production

With both relieved metabolic burdens and increased enzyme availability to enhance the naringenin biosynthesis by the tri-function circuits, a high accumulation of *p*-coumaric acid was still observed. As the naringenin synthesis requires the condensation of malonyl-CoA and *p*-coumaroyl-CoA, the limited availability of intracellular malonyl-CoA is now a major restriction for enhancing the naringenin production (Fowler et al., 2009; Leonard et al., 2008; Xu et al., 2011). As the fundamental building block for fatty acid biosynthesis, simply blocking the malonyl-CoA consumption statically was demonstrated to be harmful for cell growth as well as the naringenin biosynthesis (Yang et al., 2015; Zhou et al., 2021). The feedback or feedforward control can be conducted to balance the malonyl-CoA distribution for cell growth and naringenin biosynthesis. In our previous research, the gene *fabD* for fatty acid biosynthesis was demonstrated to be an efficient repression target for improving the availability of malonyl-CoA (Yang et al., 2015).

Thus, to further enhance the naringenin titer, the feedback control powered by the naringenin biosensor system FdeR-P_{fdeA} was integrated to dynamically enhance the malonyl-CoA supply by repressing the expression of *fabD* using anti-sense RNA *asfabD* (Fig. 5A). To achieve this, the P_{fdeA}-controlled *asfabD* transcription cassette was inserted to all three tri-function circuits enabled by different PadR regulators. However, the integration of the product-induced feedback control to three tri-function circuits all resulted in decreased naringenin titers (Fig. 5B and C). We reasoned that this was likely because the naringenin-triggered feedback control for *fabD* repression may not result in a timely repression on *fabD* expression, and the low output strength of naringenin-based biosensor system caused insufficient repression on *fabD* expression. Thus, we sought to use the *p*-coumaric acid-triggered feedforward control to regulate the *asfabD* transcription. This *p*-coumaric acid-based feedforward control can start the repression toward *fabD* gene after signaling the accumulation of *p*-coumaric acid, which can result in earlier execution of regulation compared to the naringenin-based feedback control. Moreover, the *p*-coumaric acid-responsive biosensor also exhibited high responsive strengths, which can effectively drive the asRNA transcription to repress the *fabD* expression. Thus, to this end, the P_{fdeA} promoter controlling the *asfabD* transcription was replaced by the P9 promoter (Fig. 5D), forming three finalized AutoCAD regulation systems harboring different PadR variants. The integration of the *p*-coumaric acid-induced feedforward control resulted in increased naringenin titers in all three AutoCAD regulation systems, with the highest titer (200.2 mg/L) achieved by the AutoCAD system harboring the PadR (K127Y) as regulator (Fig. 5E). We also observed a 38% decrease in *p*-coumaric acid concentration (from 713.2 to 448.7 mg/L) after the addition of the feedforward control on *asfabD* (Fig.5F). Overall, the AutoCAD regulation system, consisting of both *p*-coumaric acid-based feedforward control and naringenin-triggered feedback control, enabled relieved metabolic burdens, increased pathway efficiency, and enhanced supply of precursor, all of which contributed to a high level of naringenin production. Comparing to the initial strain without any regulation, a

16.5-fold increase (from 12.1 to 200.2 mg/L) in naringenin titer can be the achieved by applying the AutoCAD regulation system (Fig. 3B and 5E).

To further enhance the naringenin production and explore the robustness of the AutoCAD regulation system, the best engineered strain harboring the PadR (K127Y)-enabled AutoCAD regulation system was selected for fed-batch fermentation in shake flasks. By feeding 10 g/L glycerol and 5 g/L yeast extract, the highest naringenin titer, without the addition of direct precursors, reached 277.2 mg/L after 48 h (SI Appendix, Fig. S4), while the *p*-coumaric acid only accumulated to a concentration of 294.6 mg/L. The AutoCAD regulation system maintained a high naringenin production in the fed-batch fermentation. The development of AutoCAD regulation system provides valuable insights for establishing cascaded artificial dynamic control to regulate heterologous pathways. The concept of AutoCAD regulation system that contains both intermediate-based feedforward control and product-triggered feedback control can also be applied in more biosynthetic pathways to systematically and efficiently improve the pathway performance.

Discussion

Multi-function dynamic regulations are required for regulating complicated biosynthetic pathways. Nonetheless, due to the difficulties such as muti-biosensor connections and low robustness of complicated genetic circuits, only a handful of muti-layer dynamic regulations have been developed so far. In this study, we developed the AutoCAD regulation system to mimic the natural regulation in improving microbial biosynthesis. Using naringenin as the proof-of-concept demonstration, we applied the AutoCAD system to simultaneously relieve the cellular burdens, accelerate rate-limiting step, and improve precursor supply. As a result, the *de novo* naringenin titer was significantly enhanced from 12.1 mg/L to 200.2 mg/L, representing a 16.5-fold increase. Fed-batch fermentation using strain equipped with the AutoCAD system maintained the high-production phenotype and further boosted the *de novo* naringenin titer to 277.2 mg/L. These results underlined the necessity of multi-function dynamic control and validated the applicability of the AutoCAD regulation system.

While dynamic pathway regulations have been applied in naringenin biosynthesis, our AutoCAD regulation provides a more systematic approach for mimicking endogenous regulation. Compared to Zhou et al., the AutoCAD system, composed of both intermediate-triggered feedforward control and product-based feedback control, not only relieved the cellular burdens in expressing the heterologous pathways, but also dynamically improved the rate-limiting steps and increased the malonyl-CoA availability. Compared with Diah et al.'s study using the quorum sensing system, we chose metabolite-responsive biosensors in AutoCAD system which provided more specific and timely control to achieve a better production performance. The AutoCAD regulation system containing intermediate-based feedforward control and product-triggered feedback control can be applied in other biosynthesis pathways to balance the enzyme expression, enhance the rate-limiting enzyme expression, and increase the precursor supply.

As we observed in the processes of establishing the AutoCAD regulation system for improved naringenin biosynthesis, the dynamic performance of the biosensors can greatly

vary the regulation effect and enable different pathway performance. The sensitivity of the biosensor would affect the regulation timing while the responsive activity of the biosensor can influence the regulation strength. Thus, establishing biosensor libraries with versatile dynamic properties can be beneficial for constructing and applying the AutoCAD regulation systems in more biosynthetic pathways.

Supplementary Material

Refer to Web version on PubMed Central for supplementary material.

Acknowledgement

This work was supported by the National Institute of General Medical Sciences of the National Institutes of Health under award number R35GM128620. We also acknowledge the support from the College of Engineering, The University of Georgia, Athens.

References

Chouhan S, Sharma K, Zha J, Guleria S, Koffas MAG, 2017. Recent Advances in the Recombinant Biosynthesis of Polyphenols. Front Microbiol. 8, 2259. [PubMed: 29201020]

Dahl RH, Zhang F, Alonso-Gutierrez J, Baidoo E, Batth TS, Redding-Johanson AM, Petzold CJ, Mukhopadhyay A, Lee TS, Adams PD, Keasling JD, 2013. Engineering dynamic pathway regulation using stress-response promoters. Nat Biotechnol. 31, 1039–46. [PubMed: 24142050]

Dinh CV, Prather KLJ, 2019. Development of an autonomous and bifunctional quorum-sensing circuit for metabolic flux control in engineered Escherichia coli. Proc Natl Acad Sci U S A. 116, 25562–25568. [PubMed: 31796590]

Doong SJ, Gupta A, Prather KLJ, 2018. Layered dynamic regulation for improving metabolic pathway productivity in Escherichia coli. Proc Natl Acad Sci U S A. 115, 2964–2969. [PubMed: 29507236]

Farmer WR, Liao J. C. J. N. b., 2000. Improving lycopene production in Escherichia coli by engineering metabolic control. Nat Biotechnol. 18, 533–537. [PubMed: 10802621]

Fowler ZL, Gikandi WW, Koffas MAG, 2009. Increased Malonyl Coenzyme A Biosynthesis by Tuning the Escherichia coli Metabolic Network and Its Application to Flavanone Production. Appl Environ Microbiol. 75, 5831–5839. [PubMed: 19633125]

Ghofrani S, Joghataei MT, Mohseni S, Baluchnejadmojarad T, Bagheri M, Khamse S, Roghani M, 2015. Naringenin improves learning and memory in an Alzheimer's disease rat model: Insights into the underlying mechanisms. Eur J Pharmacol. 764, 195–201. [PubMed: 26148826]

Gupta A, Reizman IM, Reisch CR, Prather KL, 2017. Dynamic regulation of metabolic flux in engineered bacteria using a pathway-independent quorum-sensing circuit. Nat Biotechnol. 35, 273–279. [PubMed: 28191902]

Hengge-Aronis R, 2002. Signal transduction and regulatory mechanisms involved in control of the sigma(S) (RpoS) subunit of RNA polymerase. Microbiol Mol Biol Rev. 66, 373–395. [PubMed: 12208995]

Jiang T, Li C, Yan Y, 2021. Optimization of a p-Coumaric Acid Biosensor System for Versatile Dynamic Performance. ACS Synth Biol. 10, 132–144. [PubMed: 33378169]

Kochanowski K, Gerosa L, Brunner SF, Christodoulou D, Nikolaev YV, Sauer U, 2017. Few regulatory metabolites coordinate expression of central metabolic genes in Escherichia coli. Mol Syst Biol. 13, 903. [PubMed: 28049137]

Leonard E, Yan Y, Fowler ZL, Li Z, Lim C-G, Lim K-H, Koffas MAG, 2008. Strain Improvement of Recombinant Escherichia coli for Efficient Production of Plant Flavonoids. Molecular Pharmaceutics. 5, 257–265. [PubMed: 18333619]

Li C, Jiang T, Li M, Zou Y, Yan Y, 2021. Fine-tuning gene expression for improved biosynthesis of natural products: From transcriptional to post-translational regulation. Biotechnol Adv. 54, 107853. [PubMed: 34637919]

Li C, Zou Y, Jiang T, Zhang J, Yan Y, 2022. Harnessing plasmid replication mechanism to enable dynamic control of gene copy in bacteria. Metab Eng. 70, 67–78. [PubMed: 35033655]

Liang C, Zhang X, Wu J, Mu S, Wu Z, Jin JM, Tang SY, 2020. Dynamic control of toxic natural product biosynthesis by an artificial regulatory circuit. Metab Eng. 57, 239–246. [PubMed: 31837400]

Liu Q, Yu T, Li X, Chen Y, Campbell K, Nielsen J, Chen Y, 2019. Rewiring carbon metabolism in yeast for high level production of aromatic chemicals. Nat Commun. 10, 4976. [PubMed: 31672987]

Lucchetti-Miganeh C, Burrowes E, Baysse C, Ermel G, 2008. The post-transcriptional regulator CsrA plays a central role in the adaptation of bacterial pathogens to different stages of infection in animal hosts. Microbiology (Reading). 154, 16–29. [PubMed: 18174122]

Lutz R, Bujard H. J. N. a. r., 1997. Independent and tight regulation of transcriptional units in Escherichia coli via the LacR/O, the TetR/O and AraC/I1-I2 regulatory elements. Nucleic Acids Res. 25, 1203–1210. [PubMed: 9092630]

Lv Y, Marsafari M, Koffas M, Zhou J, Xu P, 2019. Optimizing Oleaginous Yeast Cell Factories for Flavonoids and Hydroxylated Flavonoids Biosynthesis. ACS Synth Biol. 11, 2514–2523.

Palmer CM, Miller KK, Nguyen A, Alper HS, 2020. Engineering 4-coumaroyl-CoA derived polyketide production in Yarrowia lipolytica through a beta-oxidation mediated strategy. Metab Eng. 57, 174–181. [PubMed: 31740389]

Park SC, Kwak YM, Song WS, Hong M, Yoon S. i., 2017. Structural basis of effector and operator recognition by the phenolic acid-responsive transcriptional regulator PadR. Nucleic Acids Research. 45, 13080–13093. [PubMed: 29136175]

Santos CN, Koffas M, Stephanopoulos G, 2011. Optimization of a heterologous pathway for the production of flavonoids from glucose. Metab Eng. 13, 392–400. [PubMed: 21320631]

Siedler S, Stahlhut SG, Malla S, Maury J, Neves AR, 2014. Novel biosensors based on flavonoid-responsive transcriptional regulators introduced into Escherichia coli. Metab Eng. 21, 2–8. [PubMed: 24188962]

Tani TH, Khodursky A, Blumenthal RM, Brown PO, Matthews RG, 2002. Adaptation to famine: A family of stationary-phase genes revealed by microarray analysis. Proc Natl Acad Sci U S A. 99, 13471–13476. [PubMed: 12374860]

Teng Y, Zhang J, Jiang T, Zou Y, Gong X, Yan Y, 2022. Biosensor-enabled pathway optimization in metabolic engineering. Curr Opin in Biotechnol. 75, 102696.

Wang J, Mahajani M, Jackson SL, Yang Y, Chen M, Ferreira EM, Lin Y, Yan Y, 2017. Engineering a bacterial platform for total biosynthesis of caffeic acid derived phenethyl esters and amides. Metab Eng. 44, 89–99. [PubMed: 28943460]

Wang J, Teng Y, Zhang R, Wu Y, Lou L, Zou Y, Li M, Xie Z-R, Yan Y, 2021a. Engineering a PAM-flexible SpdCas9 variant as a universal gene repressor. Nat Commun. 12, 6916. [PubMed: 34824292]

Wang J, Zhang R, Zhang J, Gong X, Jiang T, Sun X, Shen X, Wang J, Yuan Q, Yan Y, 2021b. Tunable hybrid carbon metabolism coordination for the carbon-efficient biosynthesis of 1,3-butanediol in Escherichia coli. Green Chem. 23, 8694–8706.

Wang R, Cress BF, Yang Z, Hordines JC, Zhao S, Jung GY, Wang Z, Koffas MAG, 2019. Design and characterization of biosensors for the screening of modular assembled naringenin biosynthetic library in Saccharomyces cerevisiae. ACS Synth Biol. 8, 2121–2130. [PubMed: 31433622]

Wassem R, Marin AM, Daddaoua A, Monteiro RA, Chubatsu LS, Ramos JL, Deakin WJ, Broughton WJ, Pedrosa FO, Souza EM, 2017. A NodD-like protein activates transcription of genes involved with naringenin degradation in a flavonoid-dependent manner in Herbaspirillum seropedicae. Environ Microbiol. 19, 1030–1040. [PubMed: 27878922]

Xiu Y, Jang S, Jones JA, Zill NA, Linhardt RJ, Yuan Q, Jung GY, Koffas MAG, 2017. Naringenin-responsive riboswitch-based fluorescent biosensor module for Escherichia coli co-cultures. Biotechnol Bioeng. 114, 2235–2244. [PubMed: 28543037]

Xu P, Li L, Zhang F, Stephanopoulos G, Koffas M, 2014. Improving fatty acids production by engineering dynamic pathway regulation and metabolic control. Proc Natl Acad Sci U S A. 111, 11299–304. [PubMed: 25049420]

Xu P, Ranganathan S, Fowler ZL, Maranas CD, Koffas MA, 2011. Genome-scale metabolic network modeling results in minimal interventions that cooperatively force carbon flux towards malonyl-CoA. Metab Eng. 13, 578–87. [PubMed: 21763447]

Yan Y, Kohli A, Koffas MA, 2005. Biosynthesis of natural flavanones in Saccharomyces cerevisiae. Appl Environ Microbiol. 71, 5610–3. [PubMed: 16151160]

Yang Y, Lin Y, Li L, Linhardt RJ, Yan Y, 2015. Regulating malonyl-CoA metabolism via synthetic antisense RNAs for enhanced biosynthesis of natural products. Metab Eng. 29, 217–226. [PubMed: 25863265]

Yang Y, Lin Y, Wang J, Wu Y, Zhang R, Cheng M, Shen X, Wang J, Chen Z, Li C, Yuan Q, Yan Y, 2018. Sensor-regulator and RNAi based bifunctional dynamic control network for engineered microbial synthesis. Nat Commun. 9, 3043. [PubMed: 30072730]

Zang Y, Zha J, Wu X, Zheng Z, Ouyang J, Koffas MAG, 2019. In Vitro Naringenin Biosynthesis from p-Coumaric Acid Using Recombinant Enzymes. J Agric Food Chem. 67, 13430–13436. [PubMed: 30919618]

Zhang F, Carothers JM, Keasling JD, 2012. Design of a dynamic sensor-regulator system for production of chemicals and fuels derived from fatty acids. Nat Biotechnol. 30, 354–9. [PubMed: 22446695]

Zhao J, Li C, Zhang Y, Shen Y, Hou J, Bao X, 2017. Dynamic control of ERG20 expression combined with minimized endogenous downstream metabolism contributes to the improvement of geraniol production in Saccharomyces cerevisiae. Microb Cell Factories. 16, 17.

Zhou S, Yuan SF, Nair PH, Alper HS, Deng Y, Zhou J, 2021. Development of a growth coupled and multi-layered dynamic regulation network balancing malonyl-CoA node to enhance (2S)-naringenin biosynthesis in Escherichia coli. Metab Eng. 67, 41–52. [PubMed: 34052445]

Zhou YJ, Hu Y, Zhu Z, Siewers V, Nielsen J, 2018. Engineering 1-Alkene Biosynthesis and Secretion by Dynamic Regulation in Yeast. ACS Synth Biol. 7, 584–590. [PubMed: 29284088]

Highlights

- An Autonomous Cascaded Artificial Dynamic (AutoCAD) regulation system was developed.
- AutoCAD system included both intermediate-based feedforward and product-based feedback control circuits.
- The application of AutoCAD system resulted in a 16.5-fold increase in naringenin titer.

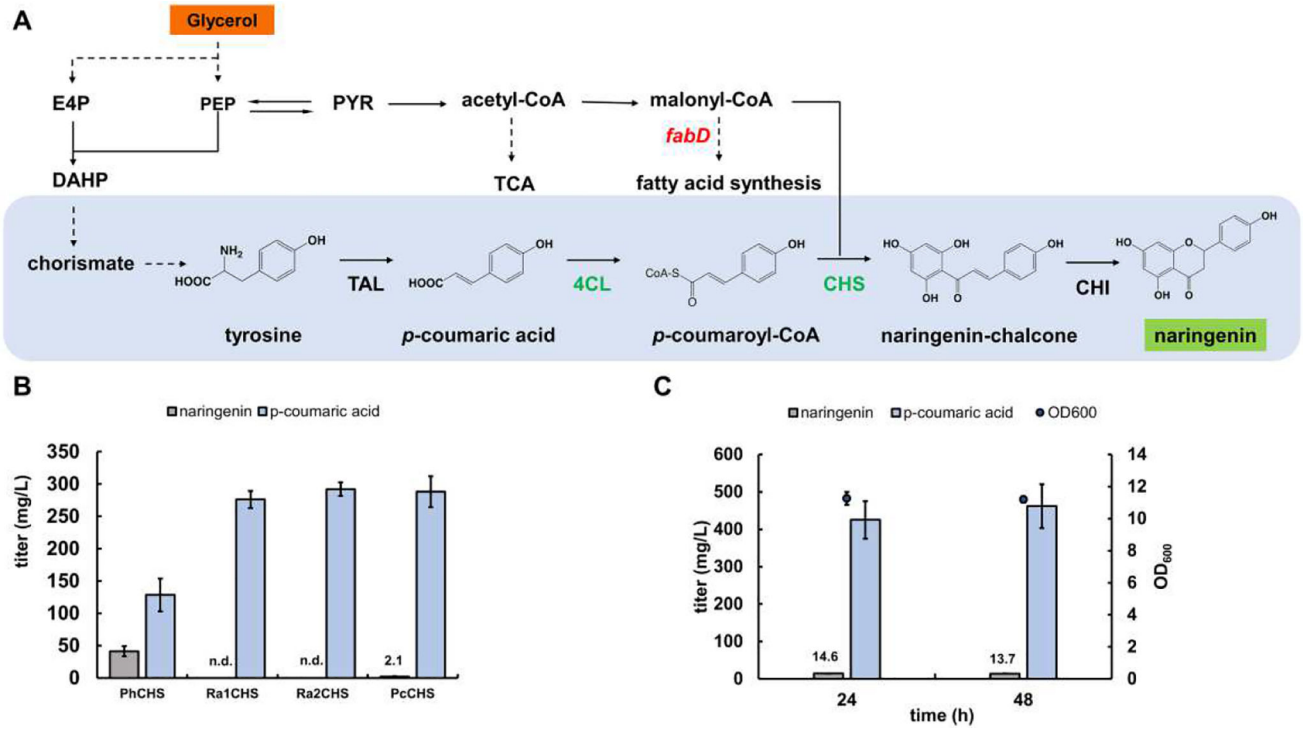

Fig. 1. Diagnosis of the issues in naringenin biosynthesis.

(**A**) Naringenin *de novo* synthesis pathway. TAL: tyrosine ammonia lyase, 4CL: 4-coumaryl-CoA ligase, CHS: chalcone synthase, CHI: chalcone isomerase. (**B**) Comparing the conversion efficiencies of different CHS by feeding 400 mg/L *p*-coumaric acid *in vivo*. (**C**) *De novo* naringenin titer and *p*-coumaric acid accumulation using the constitutively expressed pathway. All data are reported as mean±s.d. from three biologically independent experiments (n=3). Error bars are defined as s.d.

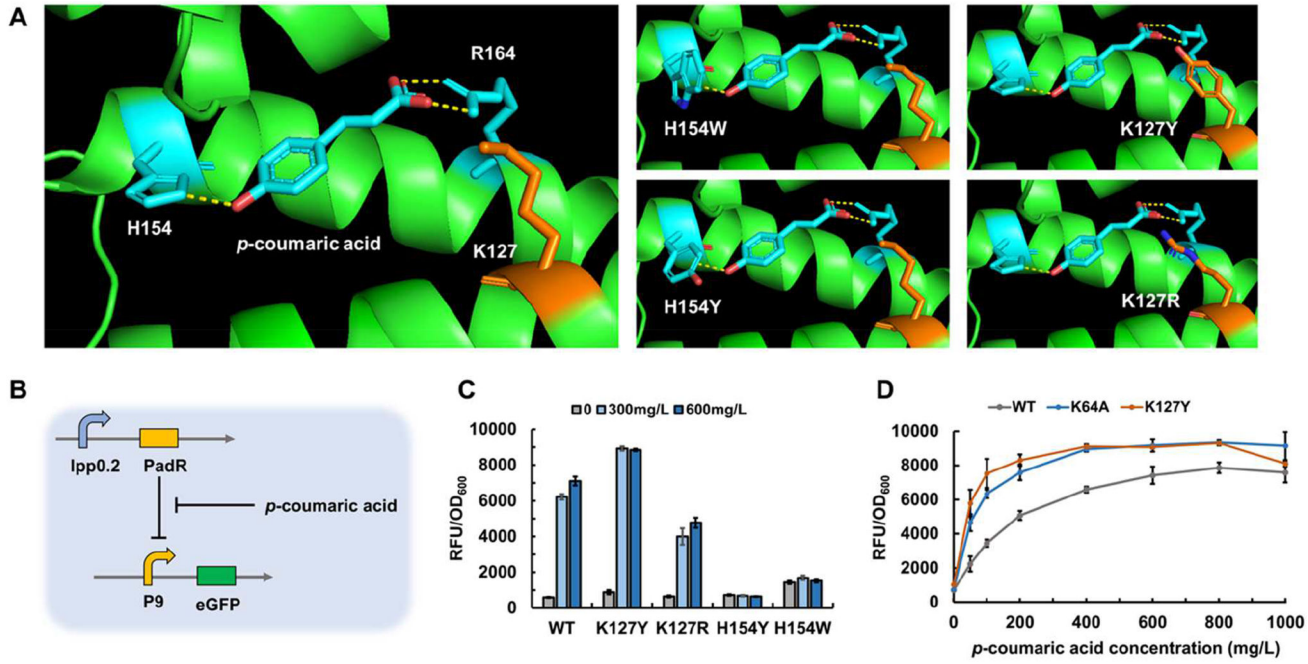

Fig. 2. Protein engineering improved the *p*-coumaric acid responsive biosensor.

(**A)** Structure simulation of PadR from *Bacillus subtilis* and its site-directed mutagenesis variants. (**B)** The mechanism of PadR-P_{padC} biosensor system. The promoter P9, a hybrid promoter, can be repressed by PadR and *p*-coumaric acid can release the inhibition. (**C)** The dynamic responsiveness of PadR variants against *p*-coumaric acid. (**D)** Dynamic ranges of PadR and its mutants under different concentrations of *p*-coumaric acid. All data are reported as mean±s.d. from three biologically independent experiments (n=3). Error bars are defined as s.d.

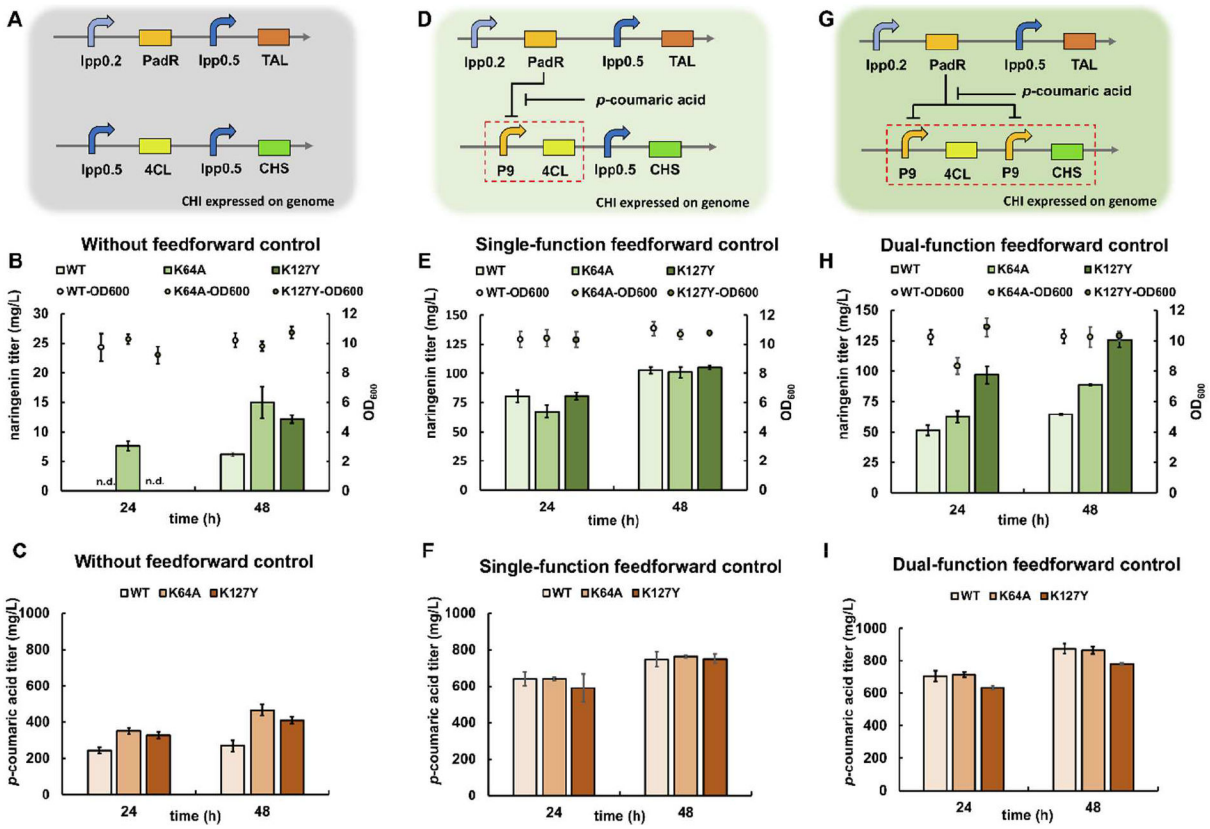

Fig. 3. Feedforward control of 4CL and CHS expression to improve naringenin production

(A) Genetic circuit without feedforward control. (**B)** The naringenin titers and cell densities when no feedforward control was applied. (**C)** The *p*-coumaric acid titers when no feedforward control was applied. (**D)** Genetic circuit of the single-function feedforward control. (**E)** The naringenin titers and cell densities when the single-function feedforward control was applied. (**F)** The *p*-coumaric acid titers when the single-function feedforward control was applied. (**G)** Genetic circuit of the dual-function feedforward control. (**H)** The naringenin titers and cell densities when the dual-function feedforward control was applied. (**I)** The *p*-coumaric acid titers when the dual-function feedforward control was applied. All data are reported as mean±s.d. from three biologically independent experiments (n=3). Error bars are defined as s.d.

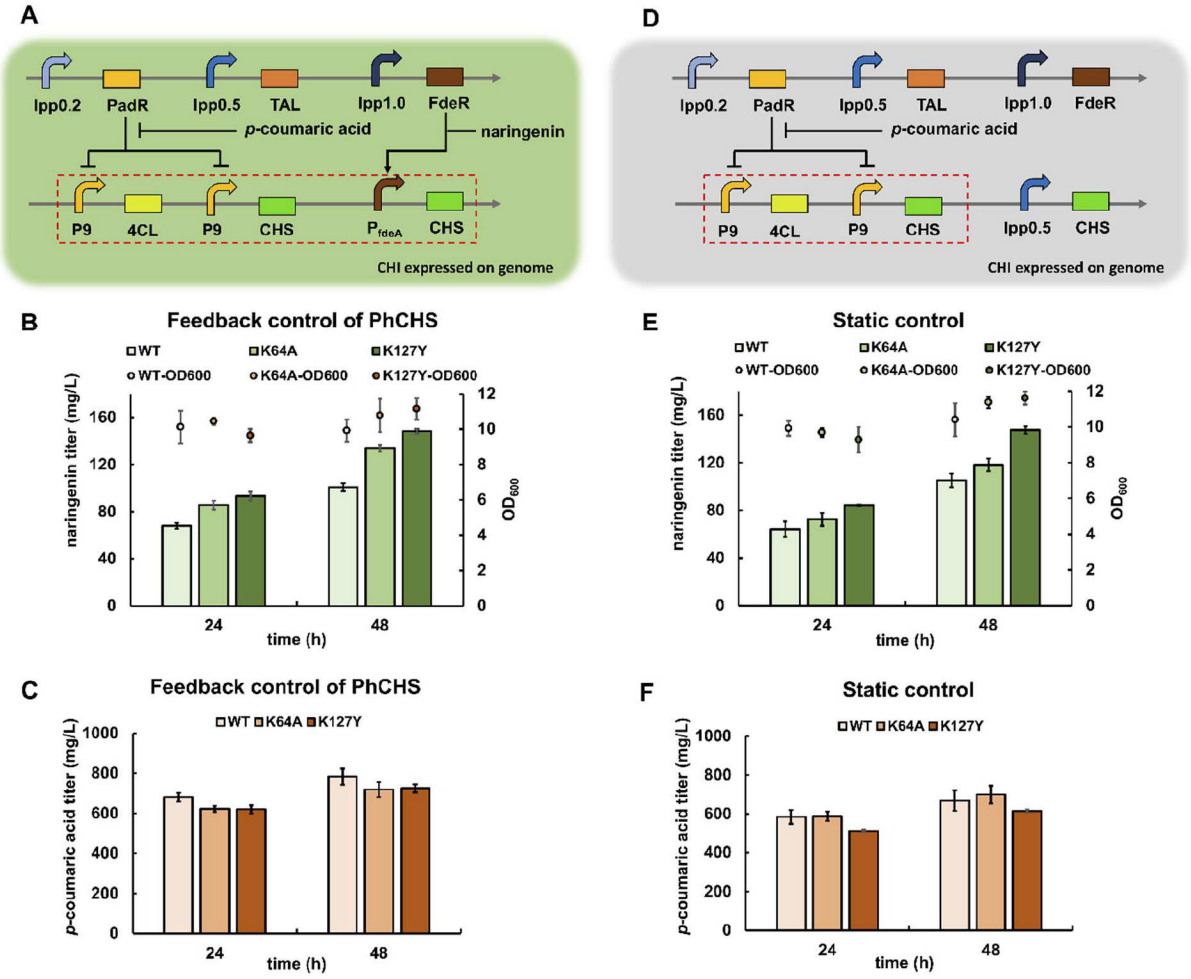

Fig. 4. Integrating feedback control to increase the expression of rate-limiting PhCHS.

(**A**) Scheme of the tri-function genetic circuits that combine both feedforward control and feedback control. (**B**) The naringenin titers and cell densities when the tri-function genetic circuits were applied. (**C**) The *p*-coumaric acid titers when the tri-function genetic circuits were applied. (**D**) Genetic circuit for the static control. Compared to the dynamic groups, the PhCHS was controlled by lpp0.5 instead of P_{fdeA}. (**E**) The naringenin titers and cell densities in static control groups. (**F**) The *p*-coumaric acid titers of static control groups. All data are reported as mean±s.d. from three biologically independent experiments (n=3). Error bars are defined as s.d.

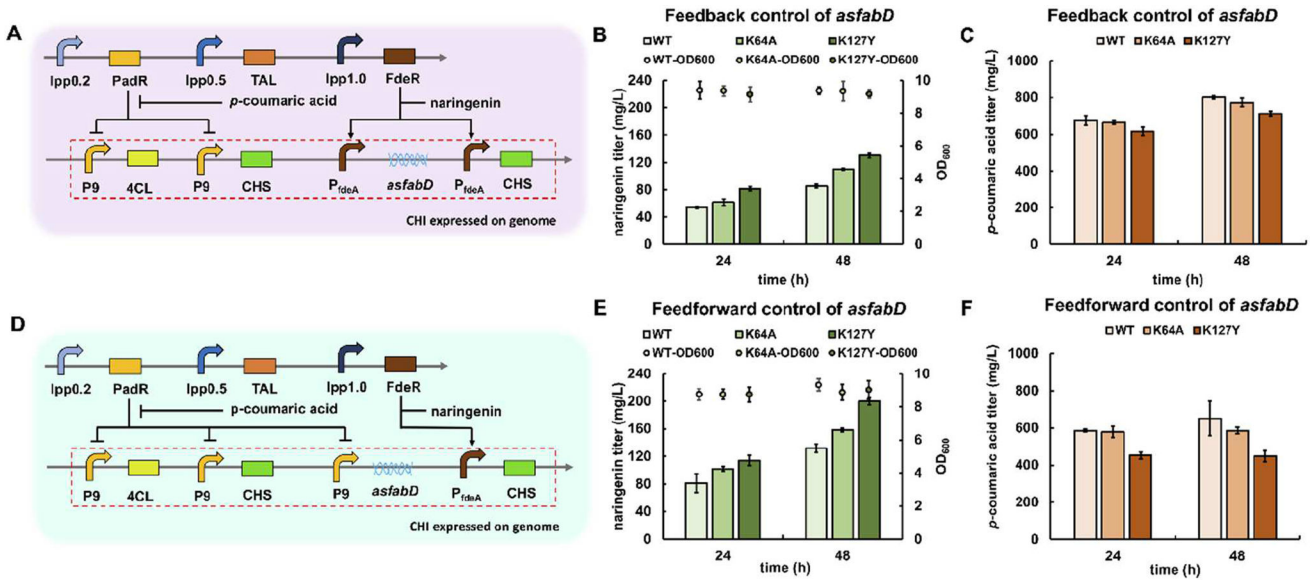

Fig. 5. Assembling the AutoCAD regulation network for improved naringenin production.

(**A)** The genetic circuit with the integration of naringenin-triggered feedback control of *asfabD*. (**B)** The naringenin titers and cell densities when *asfabD* was regulated by naringenin-triggered feedback control (**C)** The *p*-coumaric acid titers when *asfabD* was regulated by naringenin-triggered feedback control. (**D)** The genetic circuit with the integration of *p*-coumaric acid-triggered feedforward control of *asfabD* (the AutoCAD regulation system). (**E**) The naringenin titers and cell densities when the AutoCAD regulation systems were applied. (**F**) The *p*-coumaric acid titers when the AutoCAD regulation systems were applied. All data are reported as mean±s.d. from three biologically independent experiments (n=3). Error bars are defined as s.d.